$FeCl_3$ ethanol solution overnight, and then placed into the as-prepared solution, which was then mechanically stirred in the solution for around 6h with a fixed rotating speed of 300 rpm at room temperature. The sample was then taken out, washed in deionized (DI) water for 15 min, and dried in air overnight before electrochemical testing. The catalyst loading is around 4.0 mg cm^{-2}.

Preparation of IrO_2 electrode on commercial Ni foam

The IrO_2 working electrode was fabricated on Ni foam with the assistance of Nafion solution. 0.178 mmol IrO_2, 60 μL Nafion, 540 μL ethanol, and 400 μL DI water (18.3 MΩ·cm resistivity) were mixed and ultrasonicated for 30 min to prepare a homogeneous dispersion. The loading of IrO_2 catalyst on Ni foam is ~ 4.0 mg/cm^2.

Electrodeposition of NiFe layered double hydroxide (LDH) nanosheet arrays on commercial Ni foam

The electrodeposition method was similar to our previous work[1]. The electrolyte was prepared by dissolving $Ni(NO_3)_2 \cdot 6H_2O$ (0.15 M) and $FeSO_4 \cdot 7H_2O$ (0.15 M) in 100 mL water with a continuous Ar flow purging the system during electrochemical deposition in a three-electrode setup. Ni foam, Pt wire, and saturated calomel electrode (SCE) were used as the working, counter, and reference electrodes, respectively. A constant potential of -1.0 V vs SCE was applied during the electrodeposition. We can control the deposition time to deposit NiFe LDH nanosheets with a specific weight. Here the deposition time was 2.5 min. Following deposition, the samples were washed carefully by DI water for 15 min. The mass loading of NiFe LDH catalyst on Ni foam is ~ 4.0 mg/cm^2.

Synthesis of $MoNi_4/MoO_2$ cuboid arrays

To synthesize $MoNi_4$ electrocatalyst, we first grew $NiMoO_4$ cuboid arrays on commercial nickel foam via a hydrothermal procedure similar to Zhang *et al*[2]. Nickel foam was immersed into the as-prepared solution consisting of 60 ml of DI H_2O, $Ni(NO_3)_2$•$6H_2O$ (0.04 M) and $(NH_4)_6Mo_7O_{24}$•$4H_2O$ (0.01 M) in a Teflon autoclave. The autoclave was then placed in a drying oven, which was heated to 150 ^oC within 25 minutes. The growth time was 6 h. After water cleaning, the $NiMoO_4$ cuboid arrays were obtained, and were dried in air for two days before H_2 treatment. The as-obtained $NiMoO_4$ cuboid arrays were placed in a tube furnace in an Ar/H_2 (95 sccm Ar/5 sccm H_2) atmosphere. The furnace was heated to 500 ^oC and kept at 500 ^oC for 2 h. After natural cooling, the $MoNi_4/MoO_2$ cuboid arrays were obtained.

Electrochemical Testing

The OER tests were carried out in a three-electrode configuration in 1 M KOH electrolyte with high-purity oxygen purging continuously. The Ni/Fe (oxy)hydroxide sample, a Pt wire, and a mercury/mercurous oxide (Hg/HgO) reference were served as the working, counter, and reference electrodes, respectively. All of the potentials for the OER and HER were calibrated to the reversible hydrogen electrode (RHE). An average activity, which was calculated from the CV curves with the forward and backward sweeps with a very small scan rate of 1 mV s^{-1}, was utilized to evaluate the catalytic OER properties of amorphous Ni/Fe electrode activity in order to minimize the effect of capacitive current originating from the Ni-ion oxidation. This process was also applied for the overall water splitting and HER. All the other experimental conditions were very similar to our previous work[3,4].

Experimental measurements of the amount of gases generated by overall water splitting

On one hand, we utilized gas chromatography (GC) technique, which is similar to our previous work[5],

to quantify the Faraday efficiency and determine the gas species produced by the overall-water-splitting cell operating under a constant current density of 200 mA cm^{-2}. For each measurement for an interval of 10 min, 0.3 mL gas sample was carefully extracted from the sealed cell and injected into the GC instrument (GOW-MAC 350 TCD) using a glass syringe (Hamilton Gastight 1002). From this technique, we demonstrated that H_2 and O_2 were the only products with a volume ratio very close to 2:1 during water electrolysis, and the experimental gas amounts of H_2 and O_2 generated by this electrolyzer was nearly identical to the theoretical values[5]. On the other hand, in order to directly show the amount of H_2 and O_2 gases, a home-made setup was designed with two 100 mL graduated cylinders as shown below. After contacting the catalysts with the anode and cathode electrodes, we used epoxy to cover the unnecessary area of the electrodes and enameled copper wires, so that only the effective catalyst area is exposed to the electrolyte. Then each electrode was attached and fixed onto the cylinder, which was then inverted into the electrolyte vertically. The electrolysis current density was set at 500 mA cm^{-2}, and we recorded the H_2 and O_2 volumes per 10 min.

Overall water splitting driven by a thermoelectric module

A commercial thermoelectric (TE) module (bismuth telluride) was bought from Amazon. In the experiment, its hot side was covered by a large flat copper plate, which was in direct contact with a heater on top. The hot-side temperature can be maintained relatively constant by tuning the DC power supply to the heater, while the cold-side temperature can be controlled by placing it in direct contact with a cooling system, where the water inside can be adjusted to a constant temperature. Thus, the TE module can generate a relatively stable open circuit voltage between the hot and cold sides. A nano-voltmeter and an ammeter were embedded into the circuit for real-time monitoring of the voltage and current between the

working and counter electrodes of the water-splitting cell.

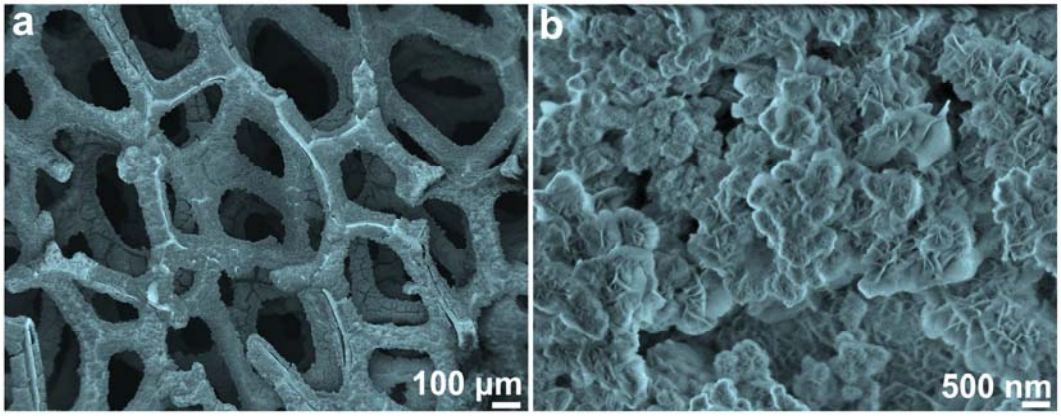

Figure S1. Typical scanning electron microscopy (SEM) images of the as-synthesized NiFe LDH nanosheet arrays on Ni foam by electrochemical deposition.

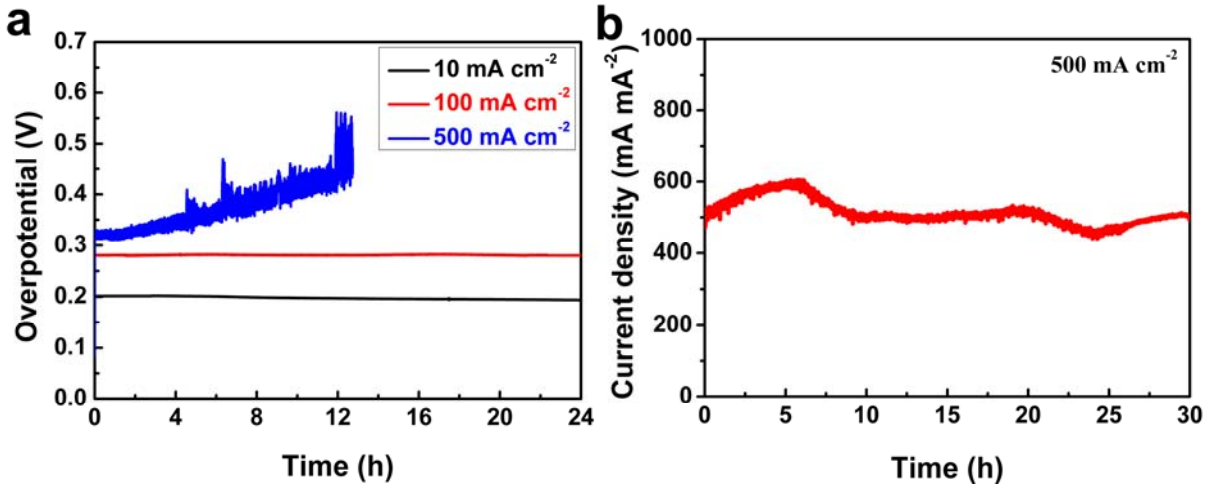

Figure S2. The durability tests of the NiFe LDH nanosheets on Cu nanowire arrays (a) and $Fe(PO_3)_2$-derived OER electrocatalsyt (b) in 1 M KOH electrolyte. It is clear to see that the former catalyst is not stable at electrolysis current of 500 mA cm^{-2}, while the latter one is stable.

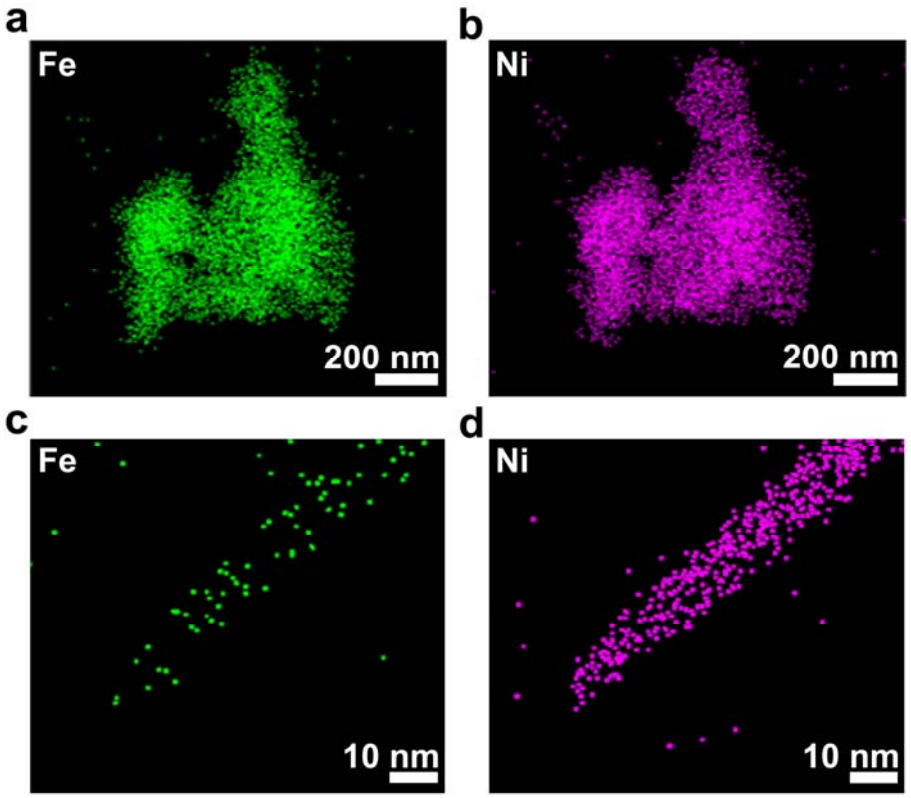

Figure S3. Elemental mapping of the Ni and Fe elements in the (Ni,Fe)OOH catalysts before (a,b) and after OER testing (c,d).

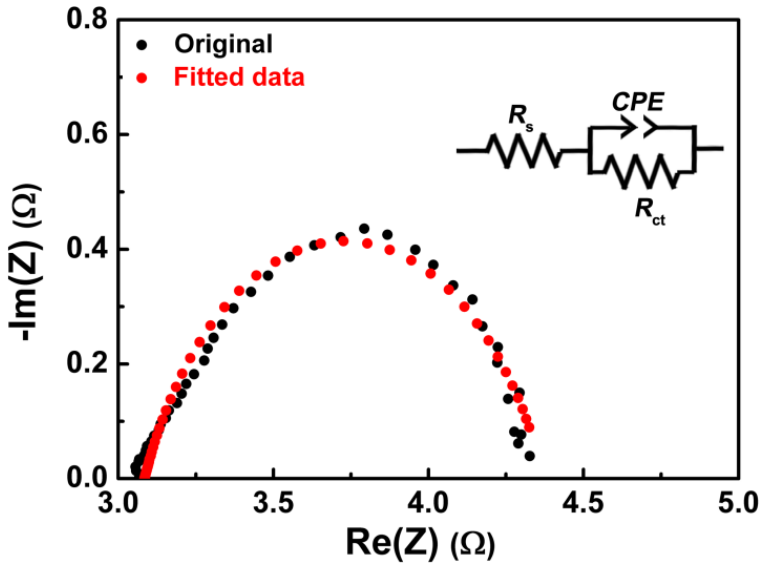

Figure S4. Nyquist plots of Ni/Fe (oxy)hydroxide electrode at the applied 300 mV overpotential in 1 M KOH electrolyte. Inset is a simplified Randle circuit model, which is used to fit the plot.

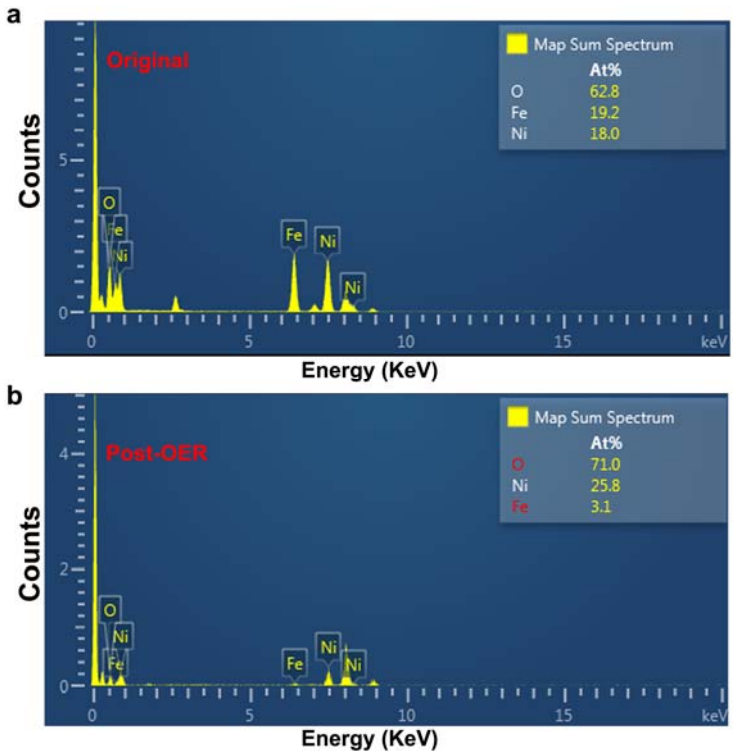

Figure S5. Typical energy-dispersive X-ray spectroscopy (EDS) spectra on the chemical compositions of original and post-OER Ni/Fe (oxy)hydroxide electrocatalysts.

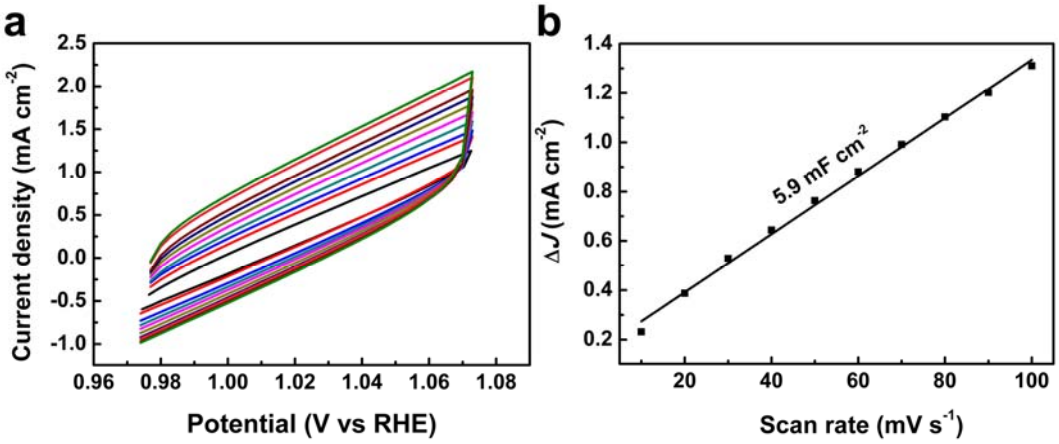

Figure S6. Double-layer capacitance (C_{dl}) measurement of the Ni/Fe (oxy)hydroxide electrode. (**a**) Typical cyclic voltammetry curves at the scan rates from 10 mV s^{-1} to 100 mV s^{-1} with a 10 mV s^{-1} interval. (**b**) Capacitive $\triangle J$ (= $J_a - J_c$) versus the scan rates. The scanning potential range is from 1.024

V to 1.124 V vs RHE.

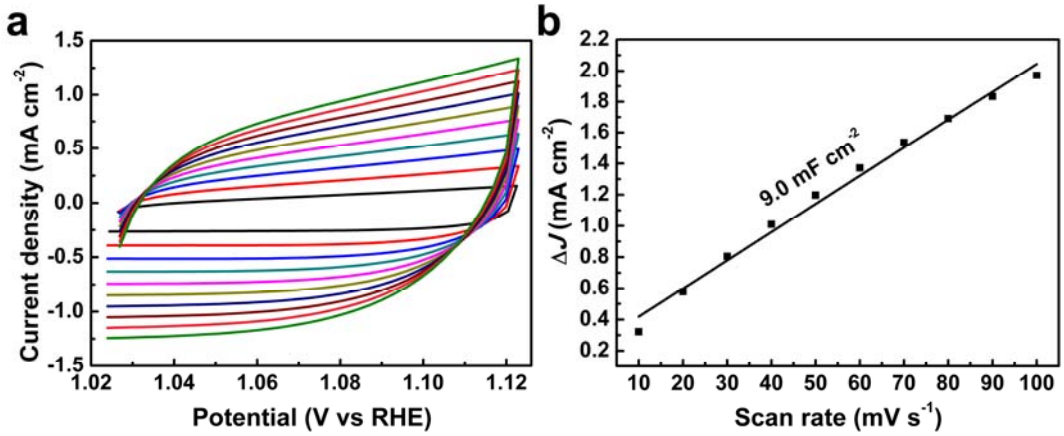

Figure S7. Double-layer capacitance (C_{dl}) measurement of the NiFe LDH electrode on Ni foam. (a) Typical cyclic voltammetry curves at the scan rates from 10 mV s^{-1} to 100 mV s^{-1} with a 10 mV s^{-1} interval. (b) Capacitive $\triangle J$ (= $J_a - J_c$) versus the scan rates. The scanning potential range is from 1.024 V to 1.124 V vs RHE.

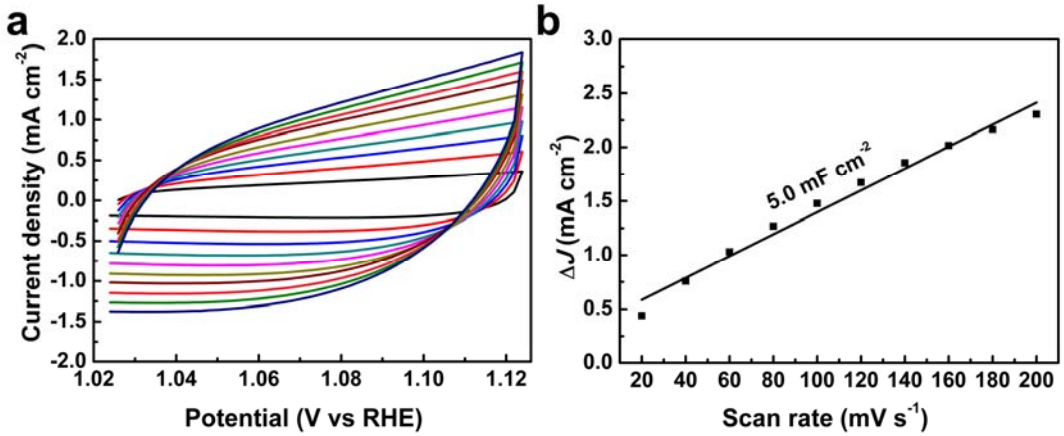

Figure S8. Double-layer capacitance (C_{dl}) measurement of the original Ni foam electrode. (a) Typical cyclic voltammetry curves at the scan rates from 20 mV s^{-1} to 200 mV s^{-1} with a 20 mV s^{-1} interval. (b) Capacitive $\triangle J$ (= $J_a - J_c$) versus the scan rates. The scanning potential range is from 1.024

V to 1.124 V vs RHE.

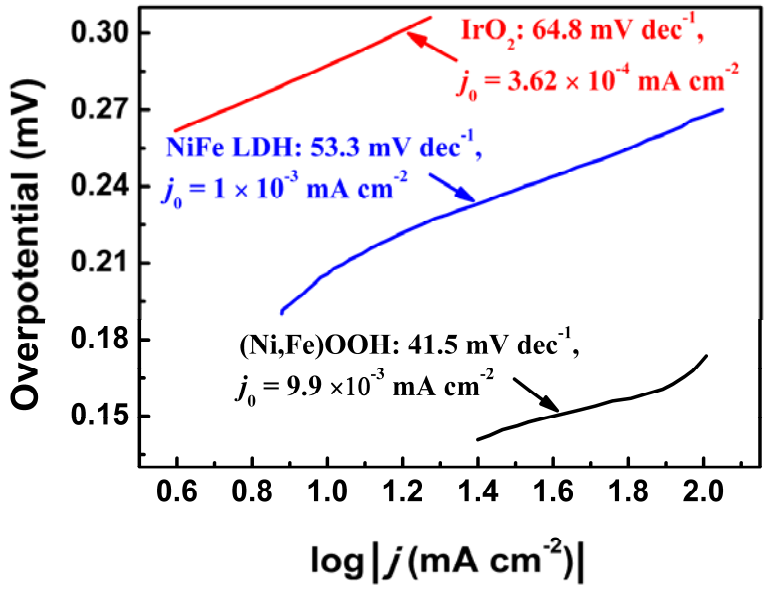

Figure S9. Tafel analysis and relevant exchange curent densities of different OER electrocatalysts in 1M KOH.

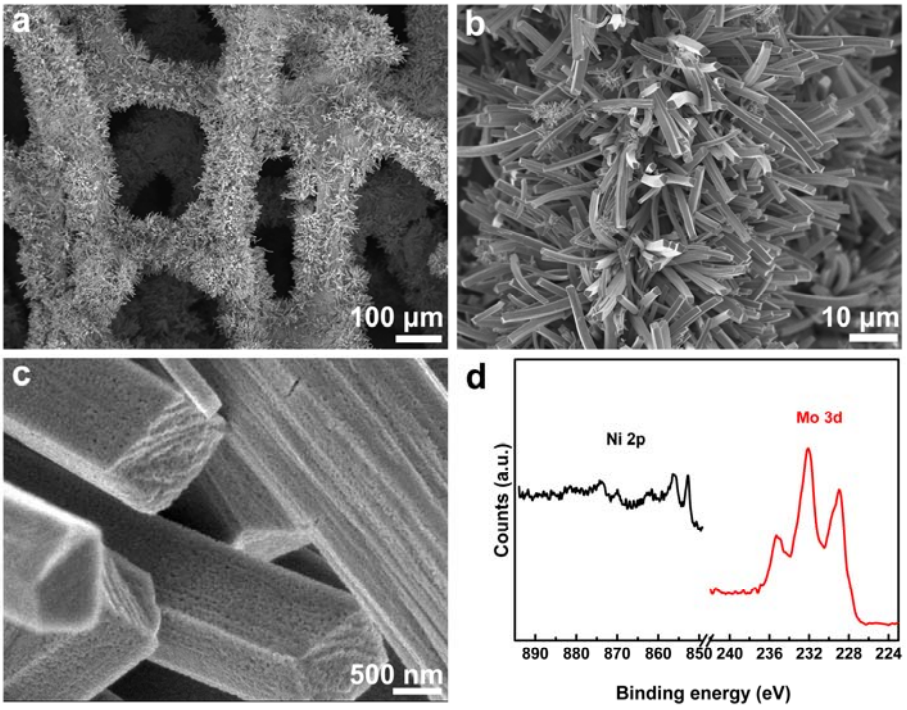

Figure S10. Characterization of an as-obtained $MoNi_4$ electrocatalyst by SEM and Raman. (**a-c**) SEM images. (**d**) XPS analysis of Ni 2p and Mo 3d binding energies.

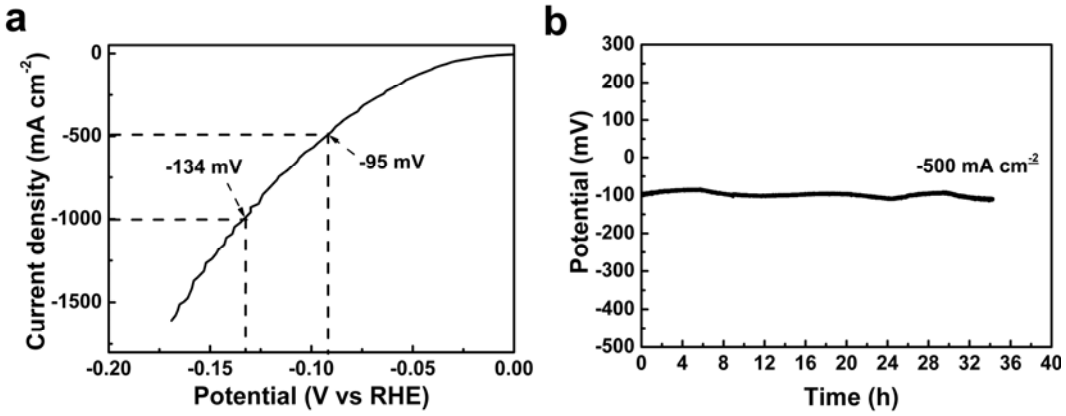

Figure S11. Hydrogen evolution catalysis by a $MoNi_4$ electrocatalyst on Ni foam. (a) Polarization curves. **(b)** Durability test at -500 mA cm^{-2} in 1M KOH electrolyte.

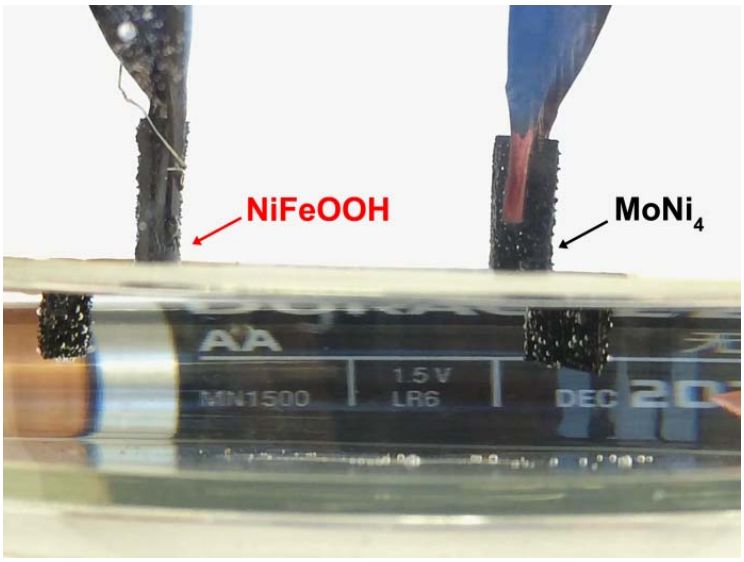

Figure S12. An optical image showing the O_2 or H_2 bubbles from overall water splitting driven by a 1.5 V AA battery.

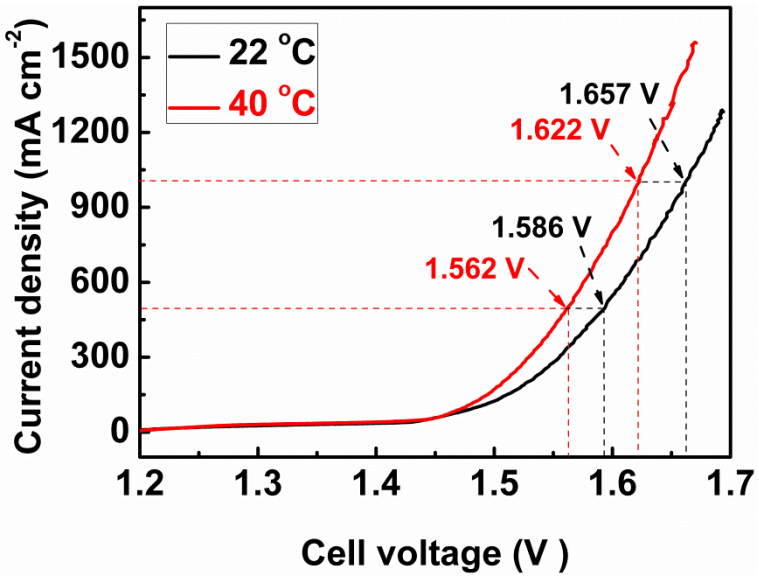

Figure S13. Enhanced overall-water-splitting activity by increasing the solution temperature to 40 °C.

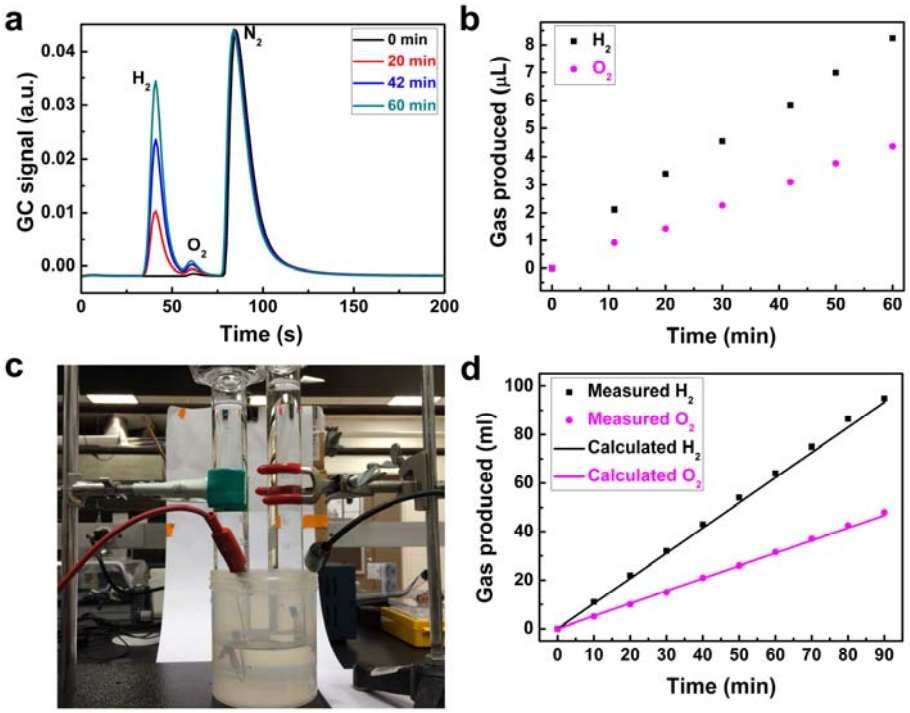

Figure S14. Experimental measurements of H_2 and O_2 gas amounts produced by our water

electrolyzer. (**a**, **b**) GC test with an injection volume of 0.3 mL. Electrolysis current density: 200 mA cm^{-2}. (**c**, **d**) Home-made setup directly testing the amount of gas by electrolysis at 500 mA cm^{-2}.

Table S1. Comparison of the catalytic OER performance between our as-constructed Ni/Fe (oxy)hydroxide catalyst and robust earth-abundant electrocatalysts reported in 1 M KOH.

Materials	**Support**	***η*@50 mA cm^{-2}**	***η*@500 mA cm^{-2}**	***j* @ 300 mV**	**Source**
Ni/Fe (oxy)hydroxide nanorod arrays	Ni foam	174 mV	259 mV	1251 mA cm^{-2}	This work
$Ni_xFe_{1-x}Se_2$-DO	Ni foam	209 mV*	283 mV*	615 mA cm^{-2}*	*ref. (6)*
Gelled FeCoW	Au foam	234 mV*	NA	167 mA cm^{-2}*	*ref. (7)*
$Fe(PO_3)_2$-derived oxyhydroxide	Ni foam	214 mV*	265 mV	1701 mA cm^{-2}	*ref. (3)*
NiFe LDH/Cu nanowire arrays	Cu foam	245 mV*	311 mV	225 mA cm^{-2}*	*ref. (1)*
NiFe LDH/r-GO	Ni foam	229 mV*	NA	286 mA cm^{-2}*	*ref. (8)*
$FeOOH/CeO_2$ nanotube arrays	Ni foam	279 mV*	NA	80 mA cm^{-2}*	*ref. (9)*
NiFe LDH/MW-graphene	Glassy carbon	335 mV*	NA	35 mA cm^{-2}*	*ref. (10)*
Fe_xN/graphene foam	Ni foam	278 mV	NA	132 mA cm^{-2}*	*ref. (4)*
NiFe LDH/CNTs	Carbon paper	272 mV*	NA	97 mA cm^{-2}*	*ref. (11)*
Co_4N nanowire arrays	Carbon cloth	308 mV*	NA	33.5 mA cm^{-2}*	*ref. (12)*
Porous MoO_2	Ni foam	297 mV*	NA	43.5 mA cm^{-2}*	*ref. (13)*
$CoNi(OH)_x$	Cu foil	313 mV*	425 mV*	35 mA cm^{-2}*	*ref (14)*
Ni_2P nanoparticles	Glassy carbon	320 mV*	NA	17 mA cm^{-2}*	*ref. (15)*
Porous Ni-P nanoplates	Glassy carbon	350 mV*	NA	11.5 mA cm^{-2}*	*ref. (16)*

h-NiS_x	Ni foam	196 mV*	~ 320 mV*	430 mA cm^{-2}*	*ref (17)*
NiFe hydroxides	Ni foam	263 mV*	NA	400 mA cm^{-2}*	*ref. (18)*

*** The value is calculated from the curves shown in the literature.**

Table S2. Summary of the electrochemical properties of porous (Ni,Fe)OOH, NiFe LDH and IrO_2 electrocatalysts on Ni foam. j_{300}, j_0 and $j_{0,\text{normalized}}$ are corresponding to the geometric current densities at 300 mV, the exchange current density and the normalized one by the relative surface area.

Catalyst	j_{300}	**Tafel slope**	C_{dl}	$j_{0,\text{geometric}}$	**Relative surface area**	$j_{0,\text{normalized}}$
(Ni,Fe)OOH	1251 mA cm^{-2}	41.5 mV dec^{-1}	5.9 mF cm^{-2}	9.9 μA cm^{-2}	1	9.9 μA cm^{-2}
NiFe LDH	293.5 mA cm^{-2}	53.3 mV dec^{-1}	9.0 mF cm^{-2}	1 μA cm^{-2}	1.53	0.835 μA cm^{-2}
IrO_2	15.5 mA cm^{-2}	64.8 mV dec^{-1}		0.362 μA cm^{-2}		

Table S3. Comparison of the overall-water-splitting activities among different earth-abundant electrocatalysts tested in 1 M KOH. V_{20}, V_{100}, V_{200}, and V_{500} correspond to the cell voltages of the overall-water-splitting cell operated at 20, 100, 200, and 500 mA cm^{-2}, respectively. $j_{1.6\text{ V}}$ represents the current density at a cell voltage of 1.6 V.

Electrolyzers	V_{50} **(V)**	V_{100} **(V)**	V_{200} **(V)**	V_{500} **(V)**	$j_{1.6\text{ V}}$ **(mA cm^{-2})**	**Source**
$NiFeOOH^{(+)}//MoNi_4^{(-)}$	1.464	1.491	1.525	1.586	585	This work
NiFe $LDH^{(+)}//Ni@Cr_2O_3^{(-)}$	1.527*	1.53*	1.57	1.670*	NA	*ref. (19)*
NiFe LDH-NS@DG $^{(+)}$//NiFe LDH-NS@DG $^{(-)}$	1.659*	1.872*	NA	NA	37.5*	*ref. (20)*
NiFe $LDH^{(+)}$//NiO/Ni-$CNT^{(-)}$	1.541*	1.584*	1.667*	NA	120*	*ref. (21)*

Porous $MoO_2^{(+)}$//Porous $MoO_2^{(-)}$	1.619*	NA	NA	NA	36*	*ref. (13)*
np-$Co_{1.04}Fe_{0.96}P^{(+)}$//np-$Co_{1.04}Fe_{0.96}P^{(-)}$	1.587*	1.615*	1.650*	1.743*	70*	*ref. (22)*
$NiFeO_x$/CFP$^{(+)}$//$NiFeO_x$/CFP$^{(-)}$	1.674*	1.73*	1.792*	NA	22*	*ref. (23)*
$Ni_{0.51}Co_{0.49}P^{(+)}$//$Ni_{0.51}Co_{0.49}P^{(-)}$	1.664*	1.71*	1.773*	NA	16*	*ref. (24)*
NiCoP$^{(+)}$//NiCoP$^{(-)}$	1.721*	1.818*	1.981*	2.37*	15*	*ref. (25)*
CoP-MNA$^{(+)}$//CoP-MNA$^{(-)}$	1.694*	1.731*	1.81*	NA	9*	*ref. (26)*
CoP$^{(+)}$//CoP$^{(-)}$	1.709*	1.745*	1.817*	NA	3*	*ref. (27)*
$NiCo_2O_4^{(+)}$//$NiCo_2O_4^{(-)}$	1.75*	NA	NA	NA	5*	*ref. (28)*
$Ni_3S_2^{(+)}$//$Ni_3S_2^{(-)}$	1.931*	NA	NA	NA	6*	*ref. (29)*
NiFe LDH/Cu nanowire arrays$^{(+)}$// NiFe LDH/Cu nanowire arrays$^{(-)}$	1.631*	1.69	1.785*	NA	32*	*ref. (1)*
h-$NiS_x^{(+)}$//h-$NiS_x^{(-)}$	1.6*	NA	NA	NA	49.5*	*ref (17)*

*** The value is calculated from the curves shown in the literature.**

References and Notes

1. Yu, L., Zhou, H. Q., Sun, J. Y., Qin, F., Yu, F., Bao, J. M., Yu, Y., Chen, S. & Ren, Z. F. Cu nanowires shelled with NiFe layered double hydroxide nanosheets as bifunctional electrocatalysts for overall water splitting. *Energy Environ. Sci.* **10**, 1820-1827 (2017).
2. Zhang, J., Wang, T., Liu, P., Liao, Z. Q., Liu, S. H., Zhuang, X. D., Chen, M. W., Zschech, E. & Feng, X. L. Efficient hydrogen production on MoNi4 electrocatalysts with fast water dissociation kinetics. *Nat. Commun.* **8**, 15437 (2017).
3. Zhou, H. Q. *et al*. Highly active catalyst derived from a 3D foam of $Fe(PO_3)_2/Ni_2P$ for extremely efficient water oxidation. *Proc. Natl. Acad. Sci. USA.* **114**, 5607-5611 (2017).

4. Yu, F., Zhou, H. Q., Zhu, Z., Sun, J. Y., He, R., Bao, J. M., Chen, S. & Ren, Z. F. Three-dimensional nanoporous iron nitride film as an efficient electrocatalyst for water oxidation. *ACS Catal.* **7**, 2052-2057 (2017).
5. Zhou, H. Q. *et al.* Efficient hydrogen evolution by ternary molybdenum sulfoselenide particles on self-standing porous nickel diselenide foam. *Nat. Commun.***7**, 12765 (2016).
6. Xu, X., Song, F. & Hu, X. L. A nickel iron diselenide-derived efficient oxygen-evolution catalyst. *Nat. Commun.***7**, 12324 (2016).
7. Zhang, B., Zheng, X. L., Voznyy, O., Comin, R., Bajdich, M., García-Melchor, M., Han, L. L., Xu, J. X., Liu, M., Zheng, L. R., Arquer, F. P. G., Dinh, C. T., Fan, F. J., Yuan, M. J., Yassitepe, E., Chen, N., Regier, T., Liu, P. F., Li, Y. H., Luna, P. D., Janmohamed, A., Xin, H. L., Yang, H. G., Vojvodic, A. & Sargent, E. H. Homogeneously dispersed multimetal oxygen-evolving catalysts. *Science* **352**, 333-337 (2016).
8. Long, X., Li, J. K., Xiao, S., Yan, K. Y., Wang, Z. L., Chen, H. N. & Yang, S. H. A strongly coupled graphene and FeNi double hydroxide hybrid as an excellent electrocatalyst for the oxygen evolution reaction. *Angew. Chem. Int. Ed.* **53**, 7584-7588 (2014).
9. Feng, J. X., Ye, S. H., Xu, H., Tong, Y. X. & Li, G. R. Design and synthesis of FeOOH/CeO_2 heterolayered nanotube electrocatalysts for the oxygen evolution reaction. *Adv. Mater.* **28**, 4698-4703 (2016).
10. Voiry, D., Yang, J., Kupferberg, J., Fullon, R., Lee, C., Jeong, H. Y., Shin, H. S. & Chhowalla, M. High-quality graphene via microwave reduction of solution-exfoliated graphene oxide. *Science* **353**, 1413-1416 (2016).

11. Gong, M., Li, Y. G., Wang, H. L., Liang, Y. Y., Wu, J. Z., Zhou, J. G., Wang, J., Regier, T., Wei, F. & Dai, H. J. An advanced Ni-Fe layered double hydroxide electrocatalyst for water oxidation. *J. Am. Chem. Soc.***135**, 8452-8455 (2013).

12. Chen, P. Z., Xu, K., Fang, Z. W., Tong, Y., Wu, J. C., Lu, X. L., Peng, X., Ding, H., Wu, C. Z. & Xie, Y. Metallic Co_4N porous nanowire arrays activated by surface oxidation as electrocatalysts for the oxygen evolution reaction. *Angew. Chem. Int. Ed.* **54**, 14710-14714 (2015).

13. Jin, Y. S., Wang, H. T., Li, J. J., Yue, X., Han, Y. J., Shen, P. K. & Cui, Y. Porous MoO_2 nanosheets as non-noble bifunctional electrocatalysts for overall water splitting. *Adv. Mater.* **28**, 3785-3790 (2016).

14. Li, S. W., Wang, Y. C., Peng, S. J., Zhang, L., Al-Enizi, A. M., Zhang, H., Sun, X. H. & Zheng, G. F. Co-Ni-based nanotubes/nanosheets as efficient water splitting electrocatalysts. *Adv. Energy Mater.* **6**, 1501661 (2016).

15. Stern, L. A., Feng, L. G., Song, F. & Hu, X. L. Ni_2P as a Janus catalyst for water splitting: the oxygen evolution activity of Ni_2P nanoparticles. *Energy Environ. Sci.* **8**, 2347-2351 (2015).

16. Yu, X. Y., Feng, Y., Guan, B. Y., Lou, X. W. & Paik, U. Carbon coated porous nickel phosphides nanoplates for highly efficient oxygen evolution reaction. *Energy Environ. Sci.* **9**, 1246-1250 (2016).

17. You, B. & Sun, Y. J. Hierarchically porous nickel sulfide multifunctional superstructures. *Adv. Energy Mater.* **6**, 1502333 (2016).

18. Lu, X. Y. & Zhao, C. Electrodeposition of hierarchically structured three-dimensional nickel-iron electrodes for efficient oxygen evolution at high current densities. *Nat. Commun.* **6**, 6616 (2015).

19. Gong, M., Zhou, W., Kenney, M. J., Kapusta, R., Cowley, S., Wu, Y. P., Lu, B. A., Lin, M. C., Wang, D. Y., Yang, J., Hwang, B. J. & Dai, H. J. Blending Cr_2O_3 into a NiO-Ni electrocatalyst for sustained water splitting. *Angew. Chem. Int. Ed.* **127**, 12157-12161 (2015).

20. Jia, Y., Zhang, L. Z., Gao, G. P., Chen, H., Wang, B., Zhou, J. Z., Soo, M. T., Hong, M., Yan, X. C., Qian, G. R., Zou, J., Du, A. J. & Yao, X. D. A heterostructure coupling of exfoliated Ni-Fe hydroxide nanosheet and defective graphene as a bifunctional electrocatalyst for overall water splitting. *Adv. Mater.* **29**, 1700017 (2017).

21. Gong, M., Zhou, W., Tsai, M. C., Zhou, J. G., Guan, M. Y., Lin, M. C., Zhang, B., Hu, Y. F., Wang, D. Y., Yang, J., Pennycook, S. J., Hwang, B. J. & Dai, H. J. Nanoscale nickel oxide/nickel heterostructures for active hydrogen evolution electrocatalysis. *Nat. Commun.* **5**, 4695 (2014).

22. Tan, Y. W., Wang, H., Liu, P., Shen, Y. H., Cheng, C., Hirata, A., Fujita, T., Tang, Z. & Chen, M. W. Versatile nanoporous bimetallic phosphides towards electrochemical water splitting. *Energy Environ. Sci.* **9**, 2257-2261 (2016).

23. Wang, H. T., Lee, H. W., Deng, Y., Lu, Z. Y., Hsu, P. C., Liu, Y. Y., Lin, D. C. & Cui, Y. Bifunctional non-noble metal oxide nanoparticle electrocatalysts through lithium-induced conversion for overall water splitting. *Nat. Commun.* **6**, 7261 (2015).

24. Yu, J., Li, Q. Q., Li, Y., Xu, C. Y., Zhen, L., Dravid, V. P. & Wu, J. S. Ternary metal phosphide with triple-layered structure as a low-cost and efficient electrocatalyst for bifunctional water splitting. *Adv. Funct. Mater.* **26**, 7644-7651 (2016).

25. Liang, H. F., Gandi, A. N., Anjum, D. H., Wang, X. B., Schwingenschlögl, U. & Alshareef, H. N. Plasma-assisted synthesis of NiCoP for efficient overall water splitting. *Nano Lett.* **16**, 7718-7725 (2016).

26. Zhu, Y. P., Liu, Y. P., Ren, T. Z. & Yuan, Z. Y. Self-supported cobalt phosphide mesoporous nanorod arrays: a flexible and bifunctional electrode for highly active electrocatalytic water reduction and oxidation. *Adv. Funct. Mater.* **25**, 7337-7347 (2015).

27. Jiang, N., You, B., Sheng, M. L. & Sun, Y. J. Electrodeposited cobalt-phosphorous-derived films as competent bifunctional catalysts for overall water splitting. *Angew. Chem. Int. Ed.* **54**, 6251-6254 (2015).

28. Gao, X. H., Zhang, H. X., Li, Q. G., Yu, X. G., Hong, Z. L., Zhang, X. W., Liang, C. D. & Lin, Z. Hierarchical $NiCo_2O_4$ hollow microcuboids as bifunctional electrocatalysts for overall water splitting. *Angew. Chem. Int. Ed.* **55**, 6290-6294 (2016).

29. Feng, L. L., Yu, G. T., Wu, Y. Y., Li, G. D., Li, H., Sun, Y. H., Asefa, T., Chen, W. & Zou, X. X. High-index faceted Ni_3S_2 nanosheet arrays as highly active and ultrastable electrocatalysts for water splitting. *J. Am. Chem. Soc.* **137**, 14023-14026 (2015).